JMEPEG (2006) 15:729-741
DOI: 10.1361/105994906X150858

1059-9495/$19.00

Cyclic Oxidation Behavior of Some Plasma-Sprayed Coatings in Na_2SO_4-60%V_2O_5 Environment

Harpreet Singh, Satya Prakash, Devendra Puri, and D.M. Phase

(Submitted February 28, 2006)

Cyclic oxidation behavior of plasma-sprayed NiCrAlY, Ni-20Cr, Ni_3Al, and Stellite-6 coatings was investigated in an aggressive environment of Na_2SO_4-60%V_2O_5 by thermogravimetric techniques for 50 cycles. These coatings were deposited on a Ni-base superalloy, namely Superni 600; 10Fe-15.5Cr-0.5Mn-0.2C-Bal Ni (wt.%). X-ray diffraction, scanning electron microscopy/energy dispersive x-ray (SEM/EDX), and electron probe microanalyzer (EPMA) techniques were used to analyze the oxidation products. The uncoated superalloy suffered accelerated oxidation in the form of intense spallation of its oxide scale. After deposition of the NiCrAlY coating, the superalloy showed a minimum mass gain, whereas after application of the Stellite-6 coating, a maximum mass gain was observed among the coatings studied. All of the coatings were found to be useful in reducing the spallation of the substrate superalloy. Moreover, the coatings were successful in maintaining continuous surface contact with the base superalloy during the cyclic oxidation. The phases revealed for the oxidized coatings were mainly the oxides of chromium and/or aluminum and the spinels containing nickel-chromium/cobalt-chromium/nickel-aluminum mixed oxides, which are reported to be protective against high-temperature oxidation/hot corrosion.

Keywords hot corrosion, NiCrAlY, plasma spray coatings, protective coatings, Stellite-6

1. Introduction

Metals and alloys are oxidized when they are heated to elevated temperatures in air or highly oxidizing environments, such as a combustion gas with an excess of air or oxygen. They often rely on the oxidation reaction to develop a protective oxide scale to resist corrosion attack, such as sulfidation, carburization, ash/salt deposit corrosion, hot corrosion, etc. That is why oxidation is considered to be the most important high-temperature corrosion reaction (Ref 1).

Nickel-base superalloys are the commercial alloys commonly used for high-temperature applications, such as manufacture of components used in aggressive environments of gas turbines and steam boilers. The superior mechanical performance and good corrosion resistance of the superalloys, especially the nickel-base superalloys at high temperature, make them favorites as base materials for hot components (such as blades or vanes) in industrial gas turbines and other energy-conversion systems. However, the presence of combustion gases and salts, such as Na_2SO_4 and V_2O_5, constitutes an extreme environment, and hot corrosion is inevitable when alloys are used at high temperatures for long periods of time (Ref 2). One protective means to counteract the problem of hot corrosion is to coat the alloy with a protective layer using various surface-treatment techniques. Several coating techniques have been suggested, such as pack cementation, plasma spraying, and chemical vapor deposition.

Among the various coating methods available, plasma spraying fosters progress in both development of materials and modern coating technology due to advances in powder and wire production. The advanced plasma technique has many advantages, such as high productivity for thick coating films of more than 100 μm and good applicability for a wide range of coating materials, including ceramic powder; furthermore, the process does not cause degradation of the mechanical properties of the alloy substrate (Ref 3, 4).

Although considerable insight has been accumulated on oxidation behavior of NiCrAlY and Ni-20Cr coatings and to some extent that of Ni_3Al coatings on Ni-base superalloys in air as well as in aggressive environments at high temperatures, but relatively less information is available on the high-temperature oxidation behavior of these coatings in the aggressive environment of a molten salt (Na_2SO_4-60%V_2O_5), which has a much lower melting point (~500 °C) than other compositions of Na_2SO_4-V_2O_5 mixtures. Sodium vanadyl vanadate ($Na_2O{\cdot}V_2O_4{\cdot}5V_2O_5$) is found to be the most common salt deposit on boiler superheaters (Ref 5), which causes severe hot corrosion of the boiler tubes. This investigation will provide vital information on the hot corrosion behavior of the plasma-sprayed Stellite-6 coating, which could be useful for exploring the possibility of the use of the Stellite-6 coating in applications where both corrosion and wear problems are encountered. Uusitalo et al. (Ref 6) have also suggested there is a need to investigate the high-temperature corrosion behavior of thermal spray-coated materials in different aggressive environments. Hodgkiess and Neville (Ref 7) opined that, because of the intrinsic properties of thermal spraying techniques, more work is needed to obtain a reliable, corrosion-resistant coating in many environments. Recent reports have also recommended

Harpreet Singh, Mechanical Engineering Department, BBSB Engineering College, Fatehgarh Sahib-140 407, India; **Satya Prakash** and **Devendra Puri,** Metallurgical and Materials Engineering Department, Indian Institute of Technology Roorkee, Roorkee-247 667, India; and **D.M. Phase,** Inter-University Consortium for DAE Facilities Indore, India. Contact e-mail: hnr97@yahoo.com.

that an improved understanding of the degradation and failure mechanisms of high-temperature coatings in the field is needed, particularly with respect to the effects of engine operation and environment on the coating performance (e.g., thermal cycling) (Ref 8). As per the views of Goward (Ref 9), complete understanding of oxide adherence is still elusive and is one of the most important areas of research, for both coatings and superalloys, to provide further advances in engine efficiency and service life.

The experimental work described herein was conducted under cyclic conditions because these conditions constitute a more realistic approach toward solving the problem of metal corrosion in actual applications, where the conditions are more or less cyclic rather than isothermal (Ref 10). Further, it is learned from the literature that relatively fewer studies are reported on hot corrosion of plasma-sprayed coatings under cyclic conditions.

2. Experimental Procedures

2.1 Coating Formulations

The substrate material selected for the current study was a Ni-based superalloy, namely, Superni 600 (similar grade to Inconel 600), which was developed by Mishra Dhatu Nigham Limited (Hyderabad, India) in rolled sheet form. The chemical composition (wt.%) of the substrate material is 10Fe-15.5Cr-0.5Mn-0.2C-Balance Ni. Specimens with dimensions of ~20 × 15 × 5 mm were cut from the sheet. The specimens were polished and grit-blasted with alumina powder (grit 60) before being plasma sprayed. A 40 kW Miller (Waltham, MA) thermal plasma spray apparatus was used to deposit the coatings. Argon was used as the powder carrying gas as well as the shielding gas. All process parameters were constant throughout the coating process and included an arc current of 700 A, arc voltage 35 V, powder flow rate 3.2 rev/min, and plasma arc gas (argon) and carrier gas (argon) pressures of 59 and 40 psi, respectively. The spraying distance was kept within a range of 90-110 mm. NiCrAlY powder was used as a bond coat before applying the final coatings of Ni-20Cr, Ni_3Al, and Stellite-6 alloy powders on the specimens, whereas a bond coat of NiCrAlY itself was selected as a coating in one case. In the case of the NiCrAlY and Ni-20Cr coatings, the color of the specimens was dull green, whereas specimens coated with Stellite-6 and Ni_3Al had a shiny gray color. Details of the coating powders are reported in Table 1, whereas porosity (2-4.5%) analyses of the as-sprayed coatings have been detailed in earlier publications of the authors (Ref 11, 12). Detailed characterizations of these coatings have appeared elsewhere (Ref 12). The cross-sectional backscattered electron images (BSEI) of

Table 1 Composition, particle size, and designation of the coating powders

Coating powder	Composition, wt.%	Particle size	Designation
Ni-22Cr-10Al-1Y (Praxair NI-343)	Cr (22), Al (10), Y (1), Ni (bal)	−45 ± 10 μm	NiCrAlY
Ni-20Cr (Praxair NI-105)	Ni (80), Cr (20)	−45 ± 5 μm	Ni-20Cr
Nickel and aluminum	Stochiometric ratio, 3:1 (Ni:Al)	Ni: 74 μm	Ni_3Al
	Ni (min. assay 99.5%) and Al (min. assay 99.7%)	Al: fine powder	
Stellite-6 (Eu Troloy)	Cr (19), C (0.7), Si (2.3), Fe (3), Ni (13.5), B (1.7), W (7.5), Mn (1 max), Co (bal)	−180 ± 53 μm	Stellite-6

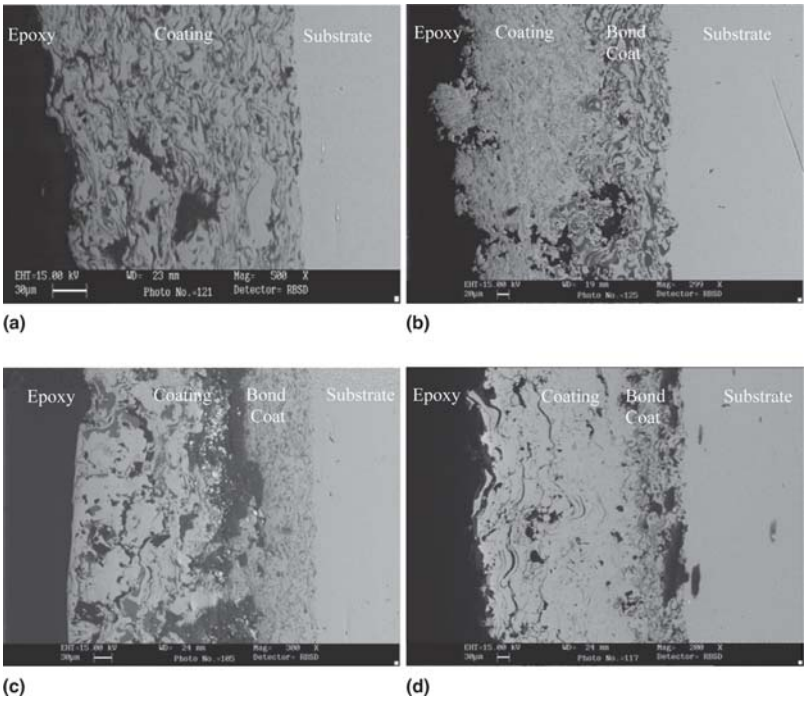

Fig. 1 BSEI micrographs showing the cross-sectional morphology of the different plasma sprayed coatings: (a) NiCrAlY coating, (b) Ni-20Cr coating with bond coat, (c) Ni_3Al coating with bond coat, and (d) Stellite-6 coating with bond coat

the as-sprayed coatings are shown in Fig. 1. The average thickness of the as-sprayed coatings was measured from these micrographs, and these measurements are listed in Table 2.

Microhardness of the as-sprayed coatings was measured with an HMV-2 series Shimadzu (Tokyo, Japan) microhardness tester. A load of 2.942 N was applied on the needle for penetration, and the hardness value was based on the relation $H_v = 0.1891 \times F/d^2$ (where F is load, in N, and d is the mean of the indentation diagonal length, in mm).

2.2 Cyclic Oxidation Studies

Cyclic oxidation studies were performed in a molten salt (Na_2SO_4-60%V_2O_5) environment for 50 cycles. Each cycle consisted of 1 h of heating at 900 °C in a silicon carbide tube furnace followed by 20 min of cooling at room temperature. Specimens were kept in alumina boats and inserted in the furnace. Studies were performed for uncoated as well as coated specimens for comparison purposes. Both coated and uncoated specimens were polished down to 1 μm alumina on a wheel cloth polisher to obtain similar conditions of reaction before the corrosion run. A layer of Na_2SO_4-60%V_2O_5 paste was applied onto preheated specimens (250 °C) with a camel-hair brush so as to have approximately 3-5 mg of paste per cm^2 of specimen surface area. Mass change measurements were taken at the end of each cycle with the help of an electronic balance (Model 06120, Contech, Mumbai, India) with a sensitivity of ±1 mg. Reproducibility in the experiments was determined by subjecting two specimens of the same alloy to the same hot corrosion test. Thermogravimetric data were analyzed to approximate the kinetics of corrosion. The oxidized specimens were subjected to x-ray diffraction (XRD), scanning electron microscopy/energy dispersive x-ray (SEM/EDX), and electron probe microanalyzer (EPMA) analyses for characterization of the corrosion products.

XRD analysis was carried out with a Bruker AXS D-8 Advance diffractometer (Karlsruhe, Germany) with Cu Kα radiation. The hot-corroded specimens were cross sectioned with an ISOMET (Buehler, Lake Bluff, IL) 1000 precision diamond cutter, mounted in transoptic mounting resin, mirror polished, and carbon coated to obtain EDX and x-ray mapping of the various elements present across the scales. SEM/EDX analysis was carried out with a JEOL (Tokyo, Japan) scanning electron microscope (JSM-5800) with an EDX attachment from Oxford (Model 6841, High Wycombe, Bucks, UK), whereas a JEOL JXA-8600M microprobe was used for taking the x-ray maps of the different elements.

Table 2 Average coating thickness of the as-sprayed coatings

	Coating thickness, μm		
Coating	**Bond coat**	**Outer coat**	**Total**
NiCrAlY	228	…	228
Ni-20Cr	155	211	366
Ni_3Al	166	247	413
Stellite-6	162	365	527

3. Results

3.1 SEM of As-Sprayed Coatings

The surface SEM images of the superalloy Superni 600 after the deposition of the plasma sprayed NiCrAlY, Ni-20Cr, Ni_3Al, and Stellite-6 coatings are shown in Fig. 2. The microstructures revealed are typical for a plasma spray process consisting of splats, which are irregularly shaped with distinct boundaries. Most of the splats are well formed without any sign of disintegration. Indications of some globules near splat boundaries can be observed in most of the micrographs; these are most likely unmelted particles. Some oxide stringers as

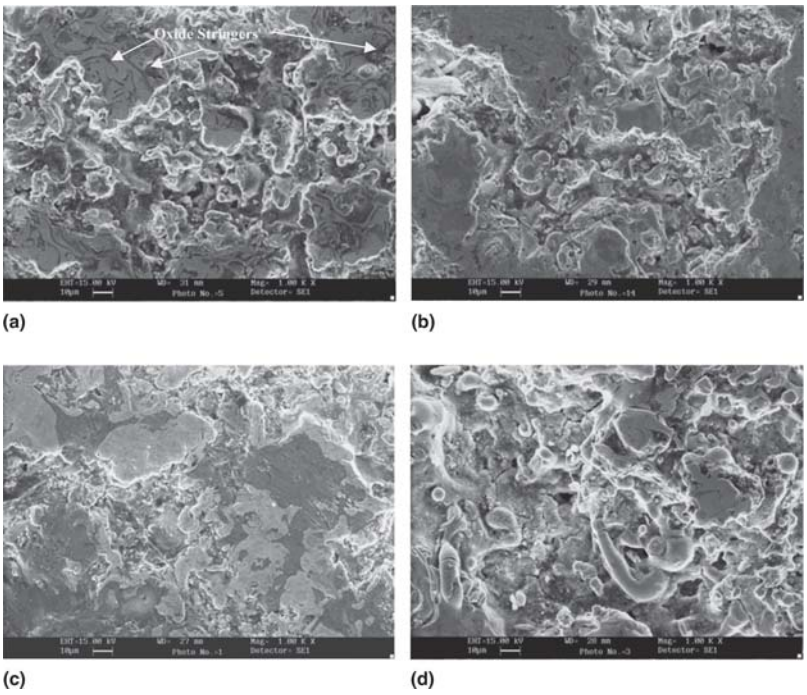

Fig. 2 Surface SEM micrographs for the plasma-sprayed coatings on the superalloy Superni 600: (a) NiCrAlY coating; (b) Ni-20Cr coating; (c) Ni_3Al coating; and (d) Stellite-6 coating

well as voids have also been noticed in general in all the coatings. Relatively speaking, the NiCrAlY and Ni-20Cr coatings have shown fine-sized splats in their structures, whereas splats are coarse in the Stellite-6 coating. Relatively medium-sized splats are formed in the Ni_3Al coating. Figure 3 depicts cross-sectional SEM micrographs of the superalloy with the different coatings.

3.2 Measurements of Microhardness of As-Sprayed Coatings

The microhardness data for the coatings are compiled in Fig. 4, which shows the microhardness profile for each coating as a function of distance from the coating-substrate interface. It is observed that the microhardness varies with the coating thickness. The microhardness of the substrate, Superni 600, has been found to be in the range of 253-350 H_v. As indicated by the profiles, the maximum value of the hardness is achieved by the Stellite-6 coating, ~487 H_v, whereas a minimum of 153 H_v is achieved by the Ni_3Al coating. Furthermore, a slight increase in the microhardness of the substrate has been observed near the coating-substrate interface in all the cases (reference points at a distance of ~40 μm).

3.3 Cyclic Oxidation in Molten Salt

The mass gain plots for uncoated and coated superalloy specimens are shown in Fig. 5, after being subjected to cyclic oxidation in an environment of Na_2SO_4-60%V_2O_5 at 900 °C for 50 cycles. In the case of the uncoated superalloy, a gray-colored scale appeared on the surfaces from the first cycle onward, which turned to dark gray as exposure progressed. The scale was fragile and tended to crack from the 17th cycle. This cracking resulted in the scale peeling up at many locations; spalling of the scale started from the 22nd cycle. This spallation continued until the end of the exposure, although with reduced magnitude.

Deposition of NiCrAlY and Ni-20Cr coatings reduced the

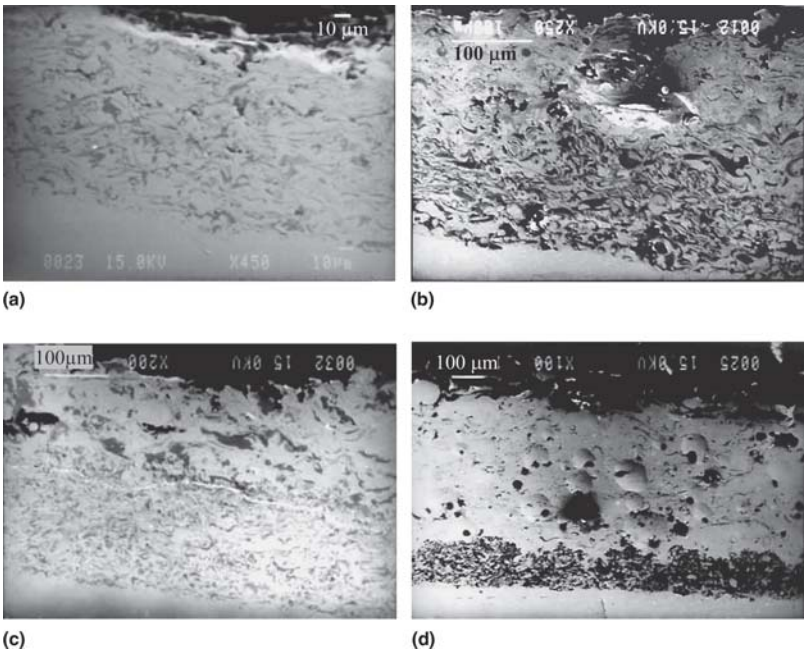

Fig. 3 SEM micrographs showing the cross-sectional morphology of the different plasma sprayed coatings: (a) NiCrAlY coating; (b) Ni-20Cr coating with bond coat; (c) Ni_3Al coating with bond coat; and (d) Stellite-6 coating with bond coat

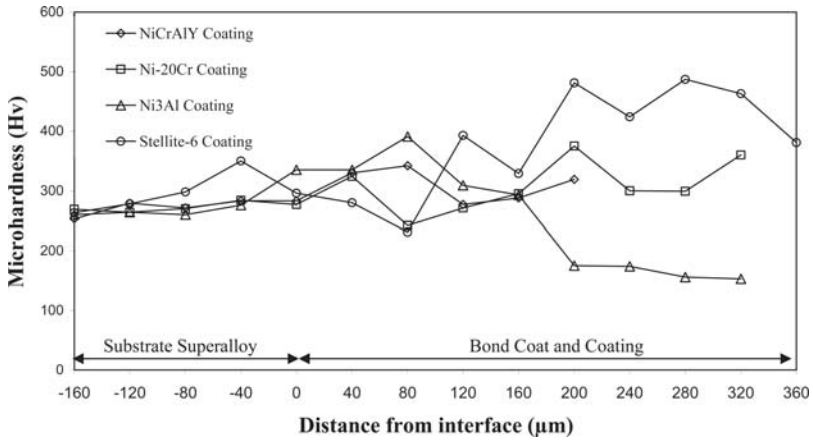

Fig. 4 Microhardness profiles for the different plasma-sprayed coatings on the superalloy Superfer 600 along the cross section

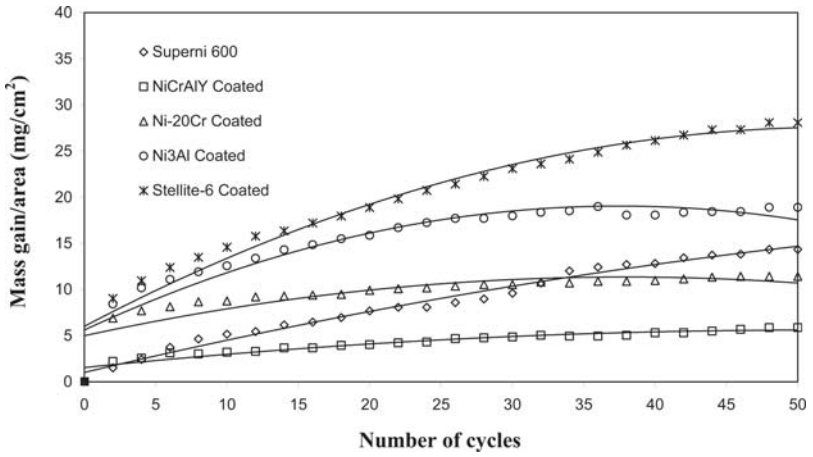

Fig. 5 Mass gain versus number of cycles plot for the coated and uncoated superalloy Superni 600 subjected to the cyclic oxidation for 50 cycles in Na_2SO_4-60%V_2O_5 at 900 °C

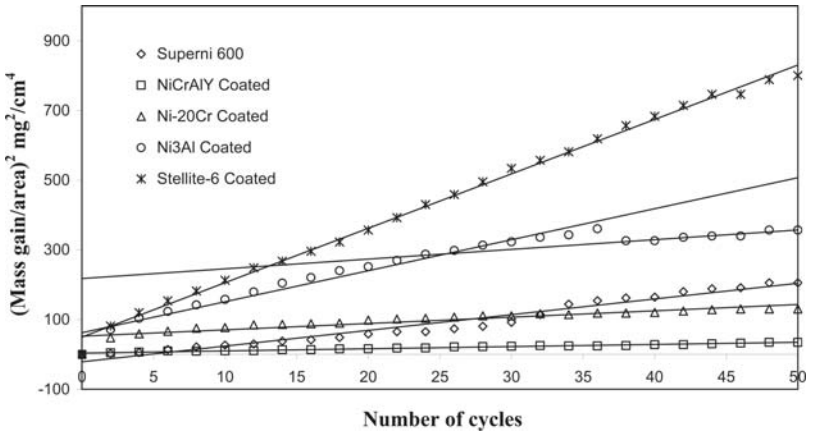

Fig. 6 (Mass gain/area)^2 versus number of cycles plot for the coated and uncoated superalloy Superni 600 subjected to cyclic oxidation for 50 cycles in Na_2SO_4-60%V_2O_5 at 900 °C

overall mass gain of the superalloy during exposure by 59 and 20%, respectively, whereas the cumulative mass gain of the superalloy was increased after application of the Ni_3Al and Stellite-6 coatings. The NiCrAlY-coated specimen showed a minimum mass gain among the investigated cases, whereas the Stellite-6 coated sample indicated a maximum mass gain that was 4.78 times that perceived by the former. The Ni-20Cr coated specimen revealed the second lowest mass gain, which was 1.95 times that of the NiCrAlY coated specimen, whereas mass gain by the Ni_3Al coating is greater than that by the NiCrAlY and Ni-20Cr coatings but is 3.22 times that achieved by the NiCrAlY coating.

The color of the oxide scale for the NiCrAlY- and Ni-20Cr-coated samples changed to dull green from dark gray with progress of the experiment, whereas the oxide scale remained green in the case of the Ni_3Al-coated superalloy. The color of the oxide scale for the Stellite-6 coated specimen was gray after the first cycle, turned to dark gray by the end of the ninth cycle, and subsequently showed formation of silver gray areas on the dark grayish background with further progress of the study. Minute superficial cracks were observed at or near some of the edges of the plasma spray-coated specimens during the first few cycles of exposure in all cases. This led to minor spallation of the coatings from the edges in the form of tiny flakes, which stopped toward the end of the exposure. However, the magnitude of this spallation was marginal, and only a few edges of the specimens were affected.

Slight spallation of the oxide scales was observed in the cases of the NiCrAlY- and Ni_3Al-coated Superni 600 in the form of green powder toward the end of exposure, whereas no such spalling was observed in the case of the Ni-20Cr-coated superalloy. Similar minor spalling of the scale was observed for the Stellite-6 coated specimen from the 11th cycle onward in the form of a fine blackish powder, which continued until the end of the study.

The oxidation rate law for the oxidized specimens was approximated by plotting the (mass gain/area)^2 data against the number of cycles, as shown in Fig. 6. Although the data shows small deviations from the parabolic rate law, the oxidation process could still be approximated by a parabolic rate law in all of the investigated cases. Table 3 shows the calculated values of the parabolic rate constant K_p for the specimens studied, ignoring minor scatter in the data.

3.4 X-Ray Diffraction Analysis

The XRD patterns of the oxidized specimens after exposure to the Na_2SO_4-60%V_2O_5 environment for 50 cycles are shown in Fig. 7 at reduced scales. The *d* values corresponding to each

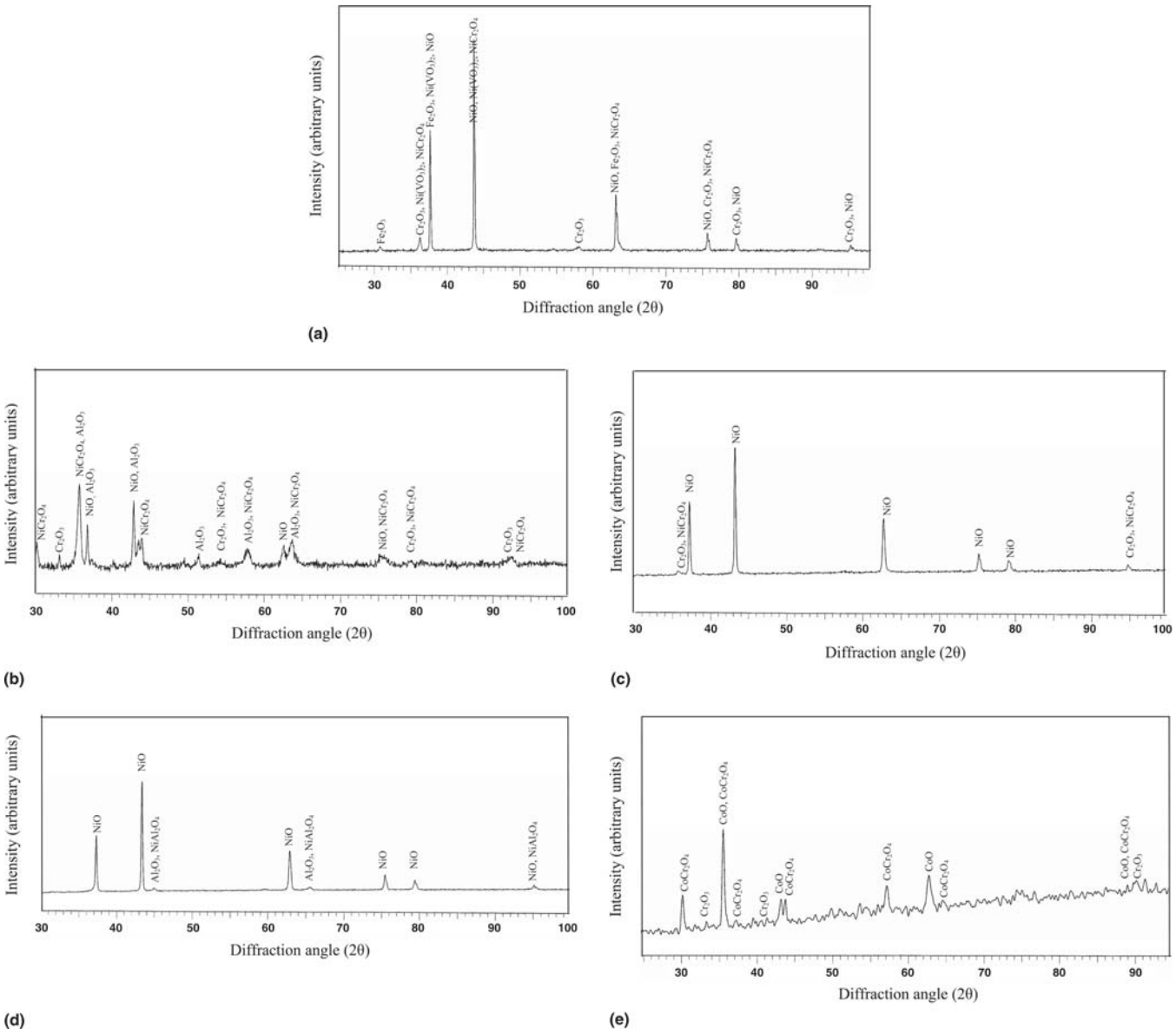

Fig. 7 XRD patterns for the superalloy Superni 600 subjected to cyclic oxidation in Na_2SO_4-60%V_2O_5 at 900 °C after 50 cycles: (a) uncoated; (b) NiCrAlY-coated; (c) Ni-20Cr coated with bond coat; (d) Ni_3Al-coated with bond coat; and (e) Stellite-6 coated with bond coat

Table 3 Values of the parabolic rate constant, K_p

Description	K_p, 10^{-10} g^2 cm^{-4} s^{-1}	R^2 value
Uncoated superalloy	12.54	0.9645
NiCrAlY-coated superalloy	1.71	0.9811
Ni-20Cr-coated superalloy	5.05	0.9610
Ni_3Al-coated superalloy	25.00 (up to 36 cycles)	0.9643
	7.74 (36 cycles and after)	0.9504
Stellite-6-coated superalloy	43.26	0.9962

peak are indicated by default by the XRD software. Analysis shows that the uncoated superalloy has NiO, $NiCr_2O_4$, Fe_2O_3, and $Ni(VO_3)_2$ phases in its scale. Deposition of the NiCrAlY, Ni-20Cr, and Ni_3Al coatings resulted in formation of NiO as the strongest phase in the oxide scale of the superalloy. Analysis for the corroded NiCrAlY-coated Superni 600 further revealed the presence of Al_2O_3 and $NiCr_2O_4$ phases. Small quantities of $NiCr_2O_4$ are also found to be present in the scale of the Ni-20Cr-coated specimen, whereas some weak peaks indicating probable formation of $NiAl_2O_4$ and Al_2O_3 are observed in the scale of the Ni_3Al-coated superalloy. The scale for the Stellite-6-coated superalloy contains CoO and $CoCr_2O_4$ phases. Relatively low-intensity peaks pertaining to Cr_2O_3 phase are also visible in the oxide scales for all of the investigated cases, except that for the Ni_3Al-coated case.

3.5 Surface Morphology of the Scales

SEM micrographs showing the surface morphology of the substrate and the coated superalloy specimens after cyclic hot corrosion for 50 cycles at 900 °C are shown in Fig. 8. One SEM micrograph (Fig. 8a) indicates a coarse-grained crystalline structure for the uncoated Superni 600, where the white phase as well as the black matrix have nearly similar compositions, with nickel and oxygen as main constituents. When deposited with the NiCrAlY coating, SEM analysis for the superalloy (Fig. 8b) reveals the presence of irregularly shaped

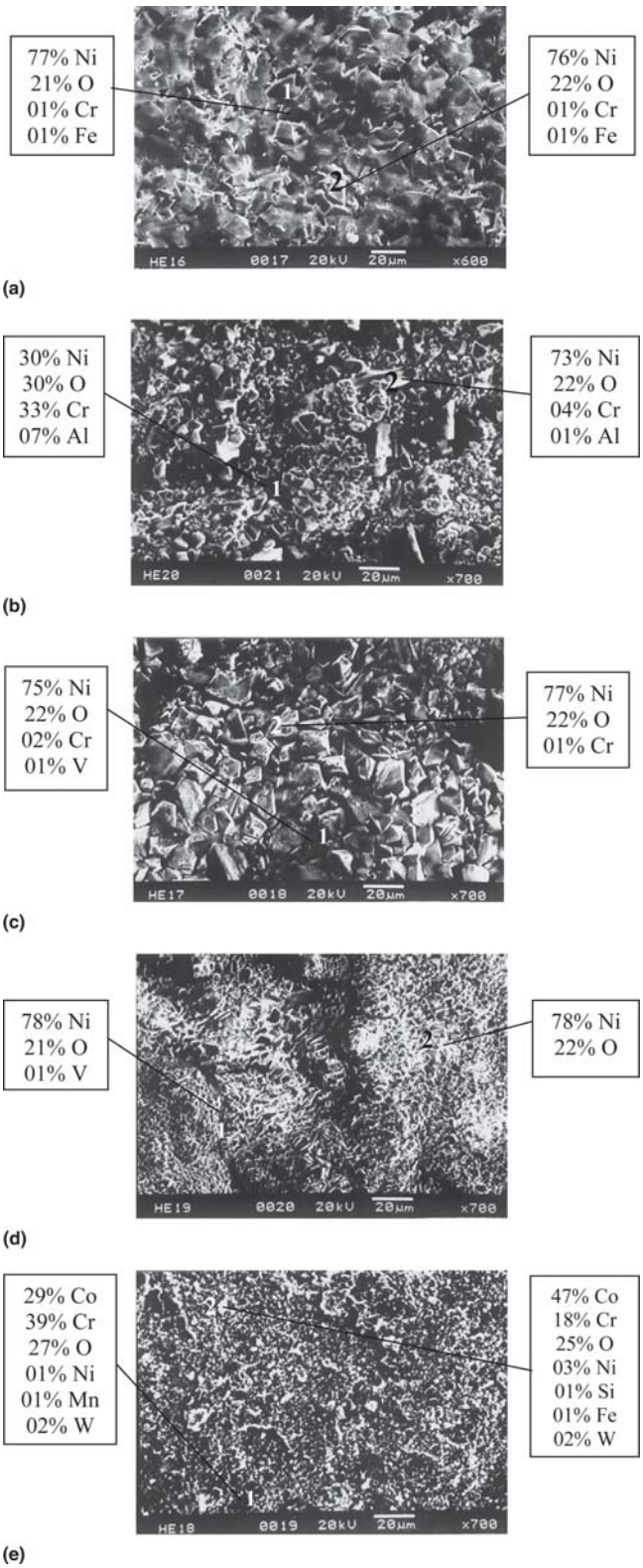

Fig. 8 Surface scale morphology and EDAX analysis (wt.%) for the superalloy Superni 600 subjected to the cyclic oxidation in Na_2SO_4-60%V_2O_5 at 900 °C: (a) uncoated, (b) NiCrAlY-coated, (c) Ni-20Cr coated with bond coat, (d) Ni_3Al-coated with bond coat, and (e) Stellite-6 coated with bond coat

crystals dispersed throughout the scale. The scale is rich in Ni and O in the upper layer; however, the subscale has nearly equal concentrations of Cr, Ni, and O. An analogous micrograph for the Ni-20Cr-coated Superni 600 (Fig. 8c) shows a blocky morphology, which is a typical structure for NiO (Ref 13). A small amount of vanadium is also present in the subscale (see point 1 in Fig. 8c). Deposition of the Ni_3Al coating resulted in a fine-grained oxide scale, where some spalling of the scale is perceptible, as revealed by the black areas in the micrograph (Fig. 8d). EDX analysis shows that the oxide scale consists mainly of Ni and O. In the case of the Stellite-6-coated Superni 600 specimen (Fig. 8e), the oxide scale contains globules distributed across its matrix, and somewhat irregularly shaped splats are seen with black color inside and a white phase along the boundaries. The white phase contains substantial concentrations of Co, O, and Cr with small quantities of Ni and W. In the black region, the amount of Co decreased substantially, but the amount of Cr doubled as compared with the white region.

3.6 Cross-Sectional Analysis of the Oxide Scales

EPMA for the oxidized Superni 600, as shown in the Fig. 9, reveals an oxide scale that is mainly nickel and iron. At most places, nickel and iron co-exist, while at other places, where chromium is present in rich concentrations, nickel and iron are absent. There is a vanadium-rich band, slightly above the scale/substrate interface, that also contains iron, nickel, and chromium. The area just below the scale/substrate interface, which represents the internal penetration zone, has mainly nickel present in it with the depletion of iron. There are some Cr-rich stringers present in this internal penetration zone, perhaps along the grain boundaries, where nickel is depleted.

EPMA analysis after deposition of the NiCrAlY coating, as shown in Fig. 10, indicates an oxide scale that has a thin outermost layer consisting mainly of chromium oxide along with some nickel and aluminum oxides. Just below this layer is an intermediate band that consists mainly of aluminum oxide. In the remaining scale, the coating has retained its original morphology, where Ni-rich and Al-rich layers are present at alternate positions. The presence of oxygen along with aluminum indicates that oxidation of the latter has taken place, whereas the Ni-rich areas are in an unreacted state. Chromium mainly co-exists with nickel, but it has also formed some clusters in the aluminum-rich areas. Vanadium and sulfur have penetrated into the scale. Furthermore, the concentration of vanadium shows a decline as one moves toward the base alloy, whereas sulfur has diffused even into the base alloy and is present mainly in the vicinity of the interface of the scale and the substrate. Iron shows some movement into the entire scale, which is more prominent near the coating-substrate interface.

A similar analysis for the cross section of the Ni-20Cr-coated Superni 600 superalloy corroded for 50 cycles in the given environment is shown in Fig. 11. From the oxygen map, it can be clearly seen that oxidation has taken place in the bond coat along the splat boundaries, where mostly aluminum and chromium are present. In the top scale, aluminum has diffused and is present in the form of the streaks, perhaps along the splat boundaries, where nickel is absent. Nickel present in the splats at some places has not oxidized, whereas in one part of the top scale, Ni and Cr, have oxidized.

An analogous analysis for the Superni 600 after deposition of the Ni_3Al coating indicates a nickel oxide-rich band at the top of the scale, which also contains dispersed aluminum oxide at places where nickel is depleted (Fig. 12). Vanadium has also diffused in this band and is present at places where both nickel

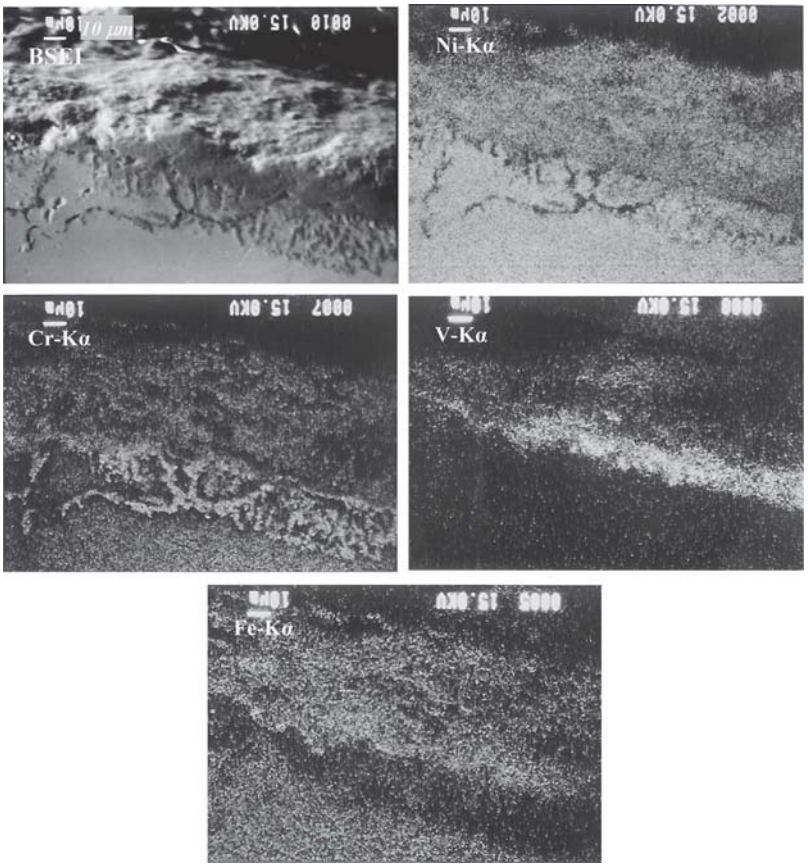

Fig. 9 BSEI and x-ray mappings of the cross section of Superni 600 subjected to cyclic oxidation in Na_2SO_4-60%V_2O_5 at 900 °C after 50 cycles

and aluminum are absent. Chromium diffusion from the bond coat into the top scale is minor. In the rest of the scale, which corresponds the bond coat, nickel-rich splats containing chromium are visible that are surrounded mainly by aluminum oxide. Chromium oxide has also formed stringers around most of these splats and co-exists with aluminum oxide. Sulfur has penetrated into the base alloy, perhaps along the grain boundaries.

EPMA analysis for the oxidized Stellite-6-coated Superni 600 superalloy depicted in Fig. 13 clearly indicates that oxygen is present along the splat boundaries in the top scale, co-existing with chromium at most places, and the splats have remained unoxidized. Similarly in the bond coat, nickel-rich splats have not suffered oxidation, and oxygen is indicated along the splat boundaries, where aluminum and chromium might have oxidized.

4. Discussion

The observed microhardness values for the as-sprayed plasma-sprayed coatings are in good agreement with those reported by Chen et al. (Ref 14), Gu et al. (Ref 15), Staia et al. (Ref 16), Liang et al. (Ref 17), Hidalgo et al. (Ref 18), Rinaldi et al. (Ref 19), Rosso et al. (Ref 20), and Sampath et al. (Ref 21). Furthermore, a slight increase in the microhardness values for the substrate superalloy observed near the interface between the bond coat and the substrate in all the cases may be attributed to the hardening of the substrate superalloy due to the high-speed impact of the coating particles during plasma spray deposition. A similar effect was also observed by Hidalgo et al. (Ref 18). The observed nonuniformity in the hardness of the coatings along the thickness may be caused by the microstructural changes along the cross section of the coatings (Ref 16). Furthermore, the microhardness and other properties of the thermal spray coatings are anisotropic due to their typical splat structure and directional solidification (Ref 22).

The uncoated Superni 600 superalloy showed intense spalling during cyclic oxidation in the given environment with a substantial mass gain. The rate of mass gain was also observed to be relatively high during the initial period of exposure, as shown in Fig. 5. Kolta et al. (Ref 23) suggested that reaction between Na_2SO_4 and V_2O_5 at 900 °C may result in formation of $NaVO_3$ (mp ≈ 610 °C) as given below:

$$Na_2SO_4 + V_2O_5 \rightarrow 2NaVO_3(l) + SO_2 + \tfrac{1}{2}O_2$$

The $NaVO_3$ acts as a catalyst and also serves as an oxygen carrier to the base alloy; therefore, it will lead to rapid oxidation of the basic elements of the superalloy to form protective oxide scales in the initial period of oxidation. However, as opined by Seiersten and Kofstad (Ref 24) and Swaminathan et al. (Ref 25), the protective oxides are disrupted or eliminated simultaneously by the molten salts, and consequently the metal surface is exposed to the direct action of an aggressive environment. For instance, Seiersten and Kofstad (Ref 24) as well as Swaminathan et al. (Ref 25) have suggested the following reaction for the dissolution of chromia scales in the molten salt:

$$Cr_2O_3 + 4NaVO_3 + \tfrac{3}{2}O_2 \rightarrow 2Na_2CrO_4(l) + 2V_2O_5$$

The hot-corroded superalloy Superni 600 showed formation of Fe_2O_3, NiO, $NiCr_2O_4$, and Ni $(VO_3)_2$ phases along with

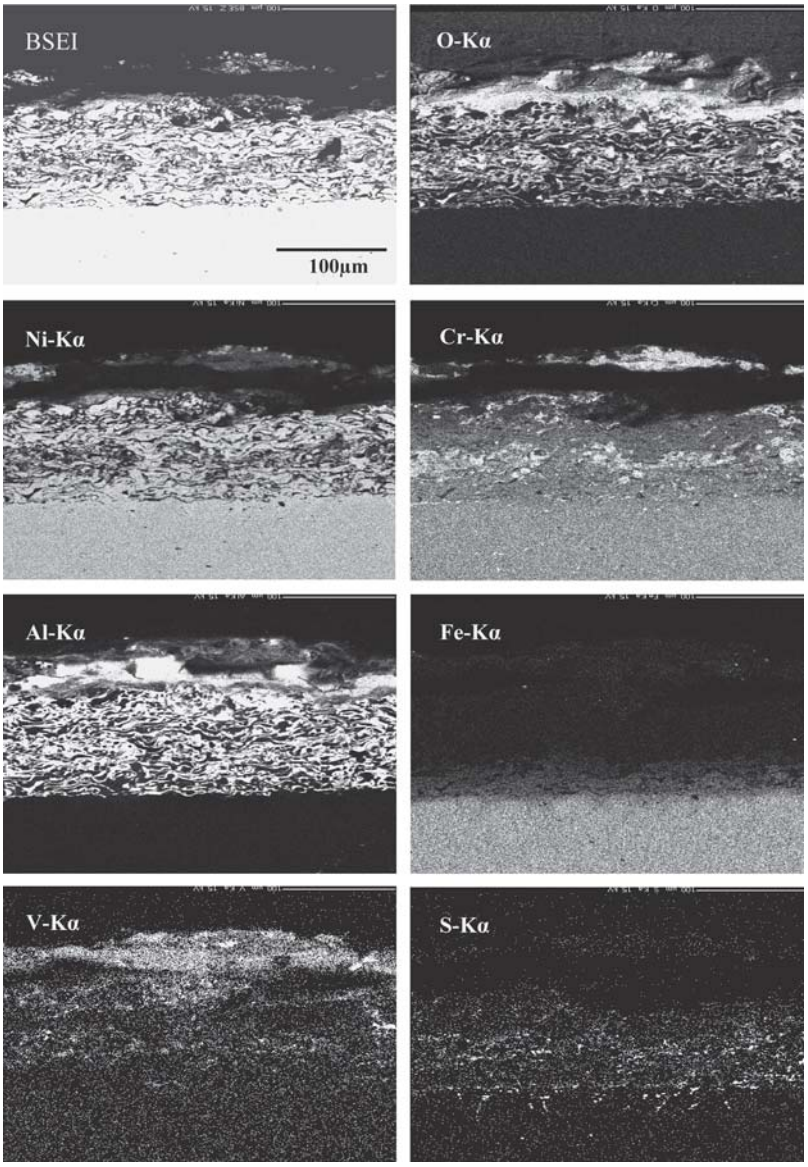

Fig. 10 BSEI and x-ray mappings of the cross section of NiCrAlY-coated superalloy Superni 600 subjected to cyclic oxidation in Na_2SO_4-60%V_2O_5 at 900 °C after 50 cycles

some weak-intensity peaks of Cr_2O_3 in its oxide scale, by XRD analysis, when subjected to the cyclic oxidation in the given environment at 900 °C. The XRD results are well supported by the SEM/EDX and EPMA results. Studies conducted by Swaminathan et al. (Ref 25), Tiwari and Prakash (Ref 26), Deb et al. (Ref 27), and Gitanjaly (Ref 28) on similar superalloys also endorse formation of identical phases. Further, the oxidized Superni 600 showed small deviations from the parabolic rate law of oxidation. Similar deviations from the parabolic rate law were also observed by Levy et al. (Ref 29) during their studies on oxidation and hot corrosion of some Ni-base advanced superalloys at 704-1093 °C.

After deposition of the NiCrAlY, Ni-20Cr, Ni_3Al, and Stellite-6 coatings, the superalloy showed relatively high mass gains in the early cycles of the oxidation in the given environment. These gains may also be attributed to the rapid formation of the oxides at the splat boundaries and open pores present in the plasma spray coatings, as the oxidizing species can easily penetrate along these splat boundaries/open pores in the early cycles of the study (Ref 30). However, once the oxides are formed at the places of the porosity and splat boundaries, the coating becomes dense, diffusion of the oxidizing species to internal portions of the coatings is slowed down, and growth of the oxides becomes limited mainly to the surface of the coated superalloy (Ref 30). This, in turn, might have made the mass gain and hence the oxidation rate steady with further progress of exposure time. In addition, the EPMA analysis as shown in Fig. 10 for the NiCrAlY-coated Superni 600 indicates that the oxide formed at these splat boundaries and within the pores is mainly aluminum oxide. Identical findings have also been reported by Bluni and Mardar (Ref 30), Choi et al. (Ref 31), and Niranatlumpong et al. (Ref 32). This aluminum oxide has been reported to be a protective oxide against hot corrosion, as it can block the diffusion paths of the oxidizing species (Ref 33).

XRD analysis for the oxidized NiCrAlY-coated Superni 600 revealed the presence of the protective oxides of nickel and aluminum and nickel-chromium spinel in the oxide scale. The EDX analysis (Fig. 8b) and the x-ray mappings (Fig. 10) also

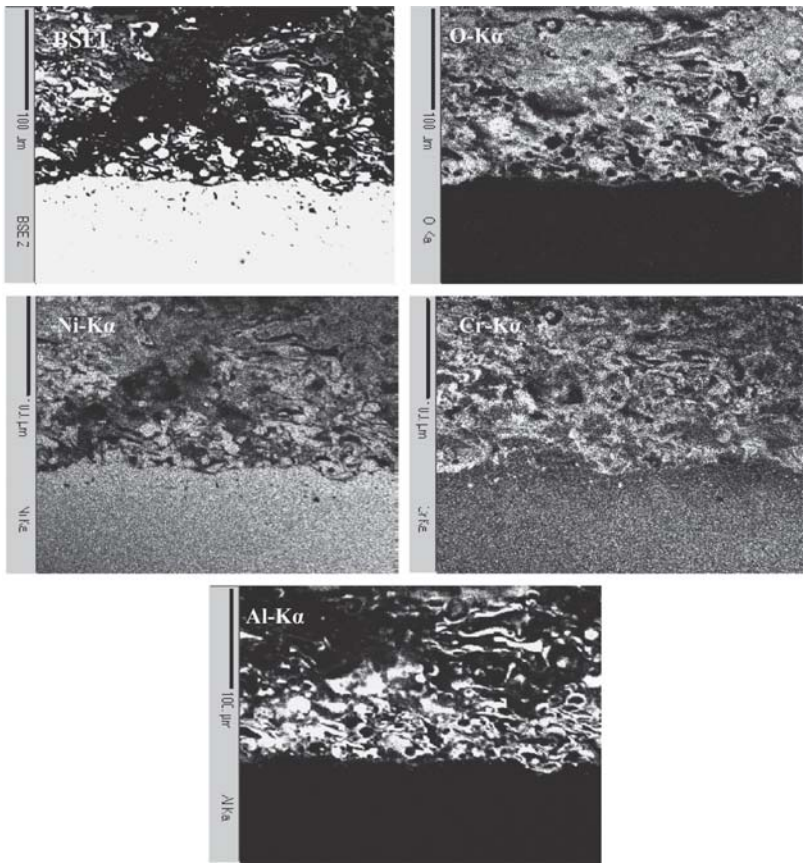

Fig. 11 BSEI and x-ray mappings of the cross section of the Ni-20Cr-coated superalloy Superni 600 subjected to cyclic oxidation in Na_2SO_4-60%V_2O_5 at 900 °C after 50 cycles

support the presence of these elements. Y. Wu et al. (Ref 34) and X. Wu et al. (Ref 35) have also reported the formation of similar phases for the NiCrAlY coatings. Longa-Nava and Takemoto (Ref 36) also identified NiO and $NiCr_2O_4$ phases along with relatively small quantities of Cr_2O_3 phase for the NiCrAl flame-sprayed coatings on steel substrates when oxidized in an environment of Na_2SO_4-85%V_2O_5 at 900 °C. They further suggested that preferential NiO and spinel formation prevent exclusive development of chromia, which is why continuous Cr_2O_3 was not present in the surface layer. This may also be the reason behind the presence of weak XRD peaks of Cr_2O_3 in the current study. These oxides, especially Al_2O_3 and Cr_2O_3, offer better protection against oxidation/hot corrosion because of their low growth rate, strongly bounded compositions, and ability to act as effective barriers against ionic migration (Ref 33). The spinel phases may further enhance the oxidation resistance with their much smaller diffusion coefficients of cations and anions than those in their parent oxides (Ref 37).

The Ni-20Cr-coated superalloy also showed formation of such phases as NiO and $NiCr_2O_4$, which is consistent with the findings of Longa-Nava et al. (Ref 38), Calvarin et al. (Ref 39), and Nickel et al. (Ref 40). Ul-Hamid (Ref 41) also reported formation of α-Cr_2O_3, $NiCr_2O_4$, and NiO phases at the surface of oxidized Ni-20 Cr alloy in different configurations. He observed the formation of an exclusive and complete α-Cr_2O_3 layer only at the localized regions, which was attributed to a slightly lower concentration of chromium in the alloy beneath the scale than the required critical level necessary to sustain such a scale throughout the alloy surface. Various regions of the oxidized alloy surface were seen to be constituted predominantly by $NiCr_2O_4$. This may be the reason behind weak peaks of Cr_2O_3 indicated in the current study. Further, Longa-Nava et al. (Ref 38) concluded from the studies on the low-pressure plasma-sprayed Ni-20Cr coatings that formation of chromate solute anions can prevent sulfidation of the alloy.

The substrate superalloy, after application of the Ni_3Al coating, showed NiO as the main XRD phase along with small amounts of Al_2O_3 in its oxide scale. Sidhu and Prakash (Ref 42) and Malik et al. (Ref 43) also reported similar phases in their oxidation studies on Ni_3Al coatings of boiler steels. The presence of NiO and $NiAl_2O_4$ phases was also observed by Lee and Lin (Ref 44) during hot corrosion studies on Ni_3Al intermetallic compounds at 800 and 1000 °C. Formation of the XRD compounds like CoO and $CoCr_2O_4$, however, as revealed in the oxide scale of the oxidized Stellite-6 coated Superni 600, is in accordance with the studies of Santoro (Ref 45) and Luthra (Ref 46). Luthra (Ref 46) proposed that formation of spinels might stop the diffusion activities through the cobalt oxide (CoO), which in turn could suppress further formation of this oxide. He further opined that an increase in the growth of $CoCr_2O_4$ and Cr_2O_3 in competition with CoO and Co_3O_4 formation enhances the corrosion resistance of alloys.

Moreover, the greenish color of the oxide scales in the case of the NiCrAlY-, Ni-20Cr-, and Ni_3Al-coated oxidized Superni 600 may be attributed to the presence of NiO as a main phase in the scale, which is identical to the findings of Bornstein et al. (Ref 47). However, the minor deviations from the parabolic

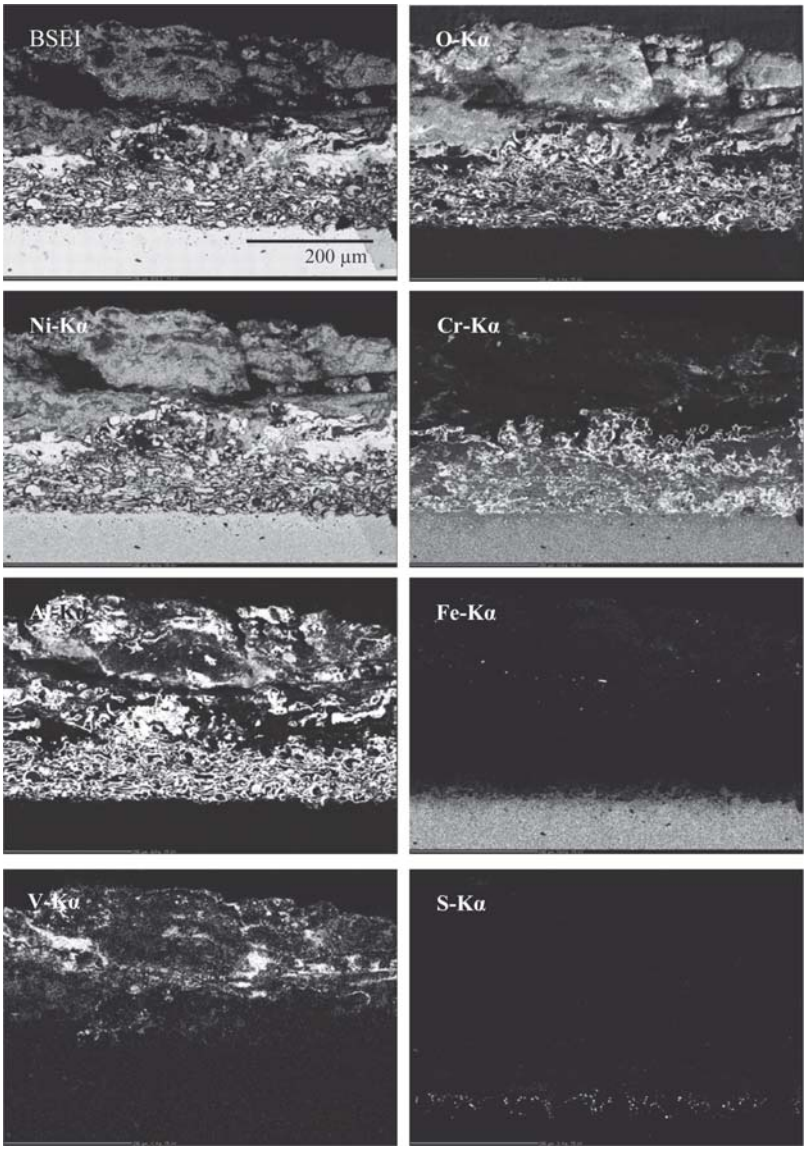

Fig. 12 BSEI and x-ray mappings of the cross section of the Ni_3Al-coated superalloy Superni 600 subjected to cyclic oxidation in Na_2SO_4-60%V_2O_5 at 900 °C after 50 cycles

rate law as shown by the coated specimens are in good agreement with the findings of Choi et al. (Ref 31) and Liu et al. (Ref 48). Choi et al. (Ref 31) attributed this scatter in data to the formation and rapid growth of inhomogeneous oxides during the oxidation process.

Furthermore, it is observed from the mass gain data (Fig. 5) that the NiCrAlY was most successful among the investigated coatings in reducing the hot corrosion rate of the superalloy, followed by the Ni-20Cr coating, whereas the oxidation rate of the Ni_3Al- and Stellite-6-coated superalloys was increased in comparison to the bare superalloy. The Stellite-6-coated superalloy showed the lowest resistance to molten salt induced oxidation among the coatings studied. This may be attributed to comparatively more spalling of coating as well as of the oxide scale observed during the exposure.

The oxide scales for the superalloy Superni 600 after deposition of the given coatings in general showed no tendency toward cracking and were found intact. This indicates further usefulness of the coatings under study as the cyclic oxidation behavior of an alloy is dictated mainly by scale spallation resistance, as per the opinion of Stott (Ref 49). However, a marginal spalling of the scales was noted in the cases of the NiCrAlY-, Ni_3Al-, and Stellite-6-coated samples. Similar spallation was also observed by Chan et al. (Ref 50) for an oxidized APS NiCrAlY coating, where it was observed that these spallation zones were invariably in the areas of local convex curvature. Strawbridge et al. (Ref 51) suggested that this spallation is associated with the development of out-of-plane tensile stresses in the region of convex curvature during cooling.

Furthermore, the plasma-sprayed NiCrAlY, Ni-20Cr, Ni_3Al, and Stellite-6 coatings were found to be successful in maintaining continuous surface contact with the base superalloy by and large, when subjected to molten salt induced oxidation. The minor cracking and subsequently small spallation of the coatings near/along the edges, as has already been mentioned, may be attributed to the thermal shocks caused by differences in the heat expansion coefficients of the oxides, coatings, and substrate (Ref 52, 53). Furthermore, the stress concentration factor at the sharp edges of the specimens might also contribute to this minor cracking and spalling.

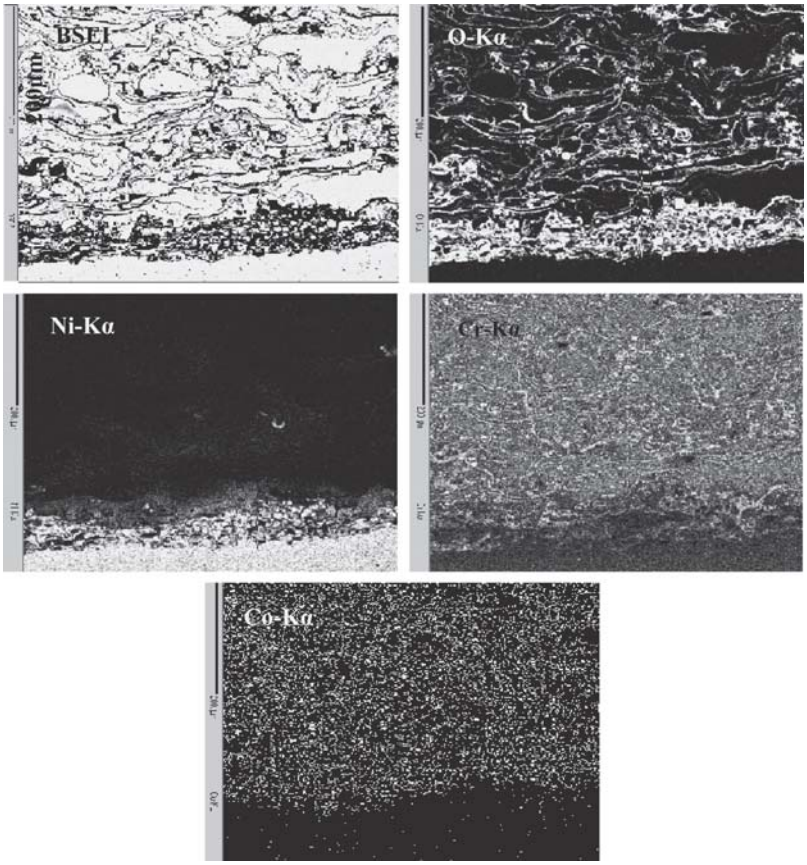

Fig. 13 BSEI and x-ray mappings of the cross-section of the Stellite-6 coated superalloy Superni 600 subjected to the cyclic oxidation in Na_2SO_4-60%V_2O_5 at 900 °C after 50 cycles.

To summarize the foregoing discussion, it can be concluded that the coatings used in this study were effective in protecting the substrate superalloy against hot corrosion in the given environment under cyclic conditions.

5. Conclusions

- For the given range of porosity and mentioned process parameters, the plasma-sprayed NiCrAlY, Ni-20Cr, Ni_3Al, and Stellite-6 coatings were found to be useful in developing resistance against cyclic oxidation in a Ni-based superalloy, namely, Superni 600 in a Na_2SO_4-60%V_2O_5 environment at 900 °C. Oxide scales after deposition of the given coatings in general showed no tendency toward cracking and were found intact. The coatings were successful in retaining adhesion with the superalloy during the cyclic oxidation. The parabolic rate law of oxidation was followed by the uncoated and the coated superalloy samples.
- Uncoated superalloy Superni 600 showed intense spallation of its oxide scale along with a substantial mass gain during the cyclic oxidation in the aggressive environment of Na_2SO_4-60%V_2O_5 at 900 °C.
- After deposition of the given coatings, the superalloy showed the presence of mainly oxides in its oxide scales when exposed to the cyclic oxidation in Na_2SO_4-60%V_2O_5 at 900 °C. The phases revealed were oxides of chromium and/or aluminum and spinels containing nickel-chromium/cobalt-chromium/nickel-aluminum type mixed oxides, which are reported to be protective against the oxidation/hot corrosion.
- Superalloy Superni 600 showed the highest resistance to cyclic oxidation in the molten salt environment after deposition of the NiCrAlY coating. The best protection indicated by the NiCrAlY coating might be attributed to the simultaneous formation of an additional protective oxide Al_2O_3, along with the Cr_2O_3 and $NiCr_2O_4$ phases, which grows very slowly and is thermodynamically stable.

Acknowledgments

The authors thankfully acknowledge the research grant from the Department of Science of Technology, Ministry of Science and Technology, New Delhi under SERC Fast Track Proposal for Young Scientists Scheme (File No. SR/FTP/ETA-06/06, dated March 16, 2006) for carrying out the R&D work on "Development of Erosion-Corrosion Resistant Thermal Spray Coatings for the Power Plant Boilers."

References

1. G.Y. Lai, *High Temperature Corrosion of Engineering Alloys,* ASM International, 1990, p 15-46
2. J.A. Goebel, F.S. Pettit, and G.W. Goward, Mechanisms for the Hot Corrosion of Nickel-Base Alloys, *Metall. Trans.,* 1973, **4,** p 261-275
3. B.J. Gill and R.C. Tucker, Jr., Plasma Spray Coating Processes, *Mater. Sci. Technol.,* 1986, **2**(3), p 207-213
4. A.R. Nicoll and G. Wahl, The Effect of Alloying Additions on M-Cr-Al-Y Systems-An Experimental Study, *Thin Solid Films,* 1983, **95,** p 21-34
5. M.M. Barbooti, S.H. Al-Madfai, and H.J. Nassouri, Thermochemical

Studies on Hot Ash Corrosion of Stainless Steel 304 and Inhibition by Magnesium Sulphate, *Thermochim. Acta,* 1988, **126,** p 43-49
6. M.A. Uusitalo, P.M.J. Vuoristo, and T.A. Mantyla, High Temperature Corrosion of Coatings and Boiler Steels in Oxidizing Chlorine-Containing Atmosphere, *Mater. Sci. Eng. A—Struct.,* 2003, **346**(1-2), p 168-177
7. T. Hodgkiess and A. Neville, An Analysis of Environmental Factors Affecting Corrosion Behavior of Thermal Spray Cermet Coatings, *Proc. 15th Int. Thermal Spray Conf.,* May 25-29, 1998 (Nice, France), ASM, 1998, Vol 1, p 63-68
8. National Materials Advisory Board, *Coatings for High-Temperature Structural Materials: Trends and Opportunities,* National Academy Press, Washington, D.C., 1996, p 1-85, available online at: http://www.nap.edu/openbook/0309053811/html
9. G.W. Goward, Progress in Coatings for Gas Turbine Airfoils, *Surf. Coat. Technol.,* 1998, **108-109,** p 73-79
10. S.E. Sadique, A.H. Mollah, M.S. Islam, M.M. Ali, M.H.H. Megat, and S. Basri, High-Temperature Oxidation Behavior of Iron-Chromium-Aluminum Alloys, *Oxid. Met.,* 2000, **54**(5-6), p 385-400
11. H. Singh, D. Puri, and S. Prakash, Some Studies on Hot Corrosion Performance of Plasma Sprayed Coatings on a Fe-Based Superalloy, *Surf. Coat. Technol.,* 2005, **192**(1), p 27-38
12. H. Singh, D. Puri, and S. Prakash, Studies of Plasma Spray Coatings on a Fe-base Superalloy, their Structure and High Temperature Oxidation Behaviour, *Anti-Corros. Methods Mater.,* 2005, **52**(2), p 84-95
13. D.F. Susan and A.R. Marder, Oxidation of Ni-Al-Base Electrodeposited Composite Coatings: I. Oxidation Kinetics and Morphology at 800° C, *Oxid. Met.,* 2002, **57**(1-2), p 131-157
14. H.C. Chen, Z.Y. Liu, and Y.C. Chuang, Degradation of Plasma-Sprayed Alumina and Zirconia Coatings on Stainless Steel During Thermal Cycling and Hot Corrosion, *Thin Solid Films,* 1993, **223**(1), p 56-64
15. Y.W. Gu, K.A. Khor, Y.Q. Fu, and Y. Wang, Functionally Graded ZrO_2-NiCrAlY Coatings Prepared by Plasma Spraying Using Premixed, Spheroidized Powders, *Surf. Coat. Technol.,* 1997, **96**(2-3), p 305-312
16. M.H. Staia, T. Valente, C. Bartuli, D.B. Lewis, and C.P. Constable, Part I: Characterization of Cr_3C_2-25% NiCr Reactive Plasma Sprayed Coatings Produced at Different Pressures, *Surf. Coat. Technol.,* 2001, **146-147,** p 553-562
17. G.Y. Liang, T.T. Wong, J.M.K. MacAlpine, and J.Y. Su, Study of Wear Resistance of Plasma-Sprayed and Laser-Remelted Coatings on Aluminium Alloy, *Surf. Coat. Technol.,* 2000, **127**(2), p 233-238
18. V.H. Hidalgo, J.B. Varela, J.M. de la Calle, and A.C. Menendez, Characterisation of NiCr Flame and Plasma Sprayed Coatings for Use in High Temperature Regions of Boilers, *Surf. Eng.,* 2000, **16**(2), p 137-142
19. C. Rinaldi, L. Ferravante, F. Uberti Paci, and P. Bianchi, Extensive Characterization of Dense and Corrosion Resistant Coatings Produced by Improved Shrouded Techniques, *Proc. Int. Thermal Spray Conf.,* May 28-30, 2001 (Singapore), ASM, 2001, p 1185-1193
20. M. Rosso, A. Scrivani, D. Ugues, and S. Bertini, Corrosion Resistance and Properties of Pump Pistons Coated with Hard Materials, *Int. J. Refract. Met. Hard Mater.,* 2001, **19,** p 45-52
21. S. Sampath, X.Y. Jiang, J. Matejicek, L. Prchlik, A. Kulkarni, and A. Vaidya, Role of Thermal Spray Processing Method on the Microstructure, Residual Stress and Properties of Coatings: An Integrated Study of Ni-5wt.%Al Bond Coats, *Mater. Sci. Eng. A—Struct.,* 2004, **364,** p 216-231
22. R.C. Tucker Jr., Advanced Thermal Spray Deposition Techniques, *Handbook of Deposition Technologies for Films and Coatings,* R.F. Bunshah, Ed., Noyes Publishers, Park Ridge, NJ, 1994, Ch 11, p 591
23. G.A. Kolta, L.F. Hewaidy, and N.S. Felix, Reactions Between Sodium Sulphate and Vanadium Pentoxide, *Thermochim. Acta,* 1972, **4,** p 151-164
24. M. Seiersten and P. Kofstad, The Effect of SO_3 on Vanadate-Induced Hot Corrosion, *High Temp. Technol.,* 1987, **5**(3), p 115-122
25. J. Swaminathan, S. Raghavan, and S.R. Iyer, Studies on the Hot Corrosion of Some Nickel-Base Superalloys by Vanadium Pentoxide, *T. Indian I. Metals,* 1993, **46**(3), p 175-181
26. S.N. Tiwari and S. Prakash, Studies on the Hot Corrosion Behaviour of Some Superalloys in Na_2SO_4-V_2O_5, *Proc. SOLCEC,* Jan 22-24, 1997 (Kalpakkam, India), IGCAR, 1997, Paper C33
27. D. Deb, S.R. Iyer, and V.M. Radhakrishnan, A Comparative Study of Oxidation and Hot Corrosion of a Cast Nickel Base Superalloy in Different Corrosive Environments, *Mater. Lett.,* 1996, **29,** p 19-23
28. Gitanjaly, "Role of Inhibitors on Hot Corrosion of Superalloys in Na_2SO_4-V_2O_5 Environment," Ph.D. Thesis, Metallurgical and Materials Engineering Department, Indian Institute of Technology Roorkee, Roorkee, India, 2003
29. M. Levy, R. Huie, and F. Pettit, Oxidation and Hot Corrosion of Some Advanced Superalloys at 1300 to 2000 °F (704 to 1093 °C), *Corrosion,* 1989, **45**(8), p 661-674
30. S.T. Bluni and A.R. Mardar, Effects of Thermal Spray Coating Composition and Microstructure on Coating Response and Substrate Protection at High Temperatures, *Corrosion,* 1996, **52**(3), p 213-218
31. H. Choi, B. Yoon, H. Kim, and C. Lee, Isothermal Oxidation of Air Plasma Spray NiCrAlY Bond Coatings, *Surf. Coat. Technol.,* 2002, **150**(2-3), p 297-308
32. P. Niranatlumpong, C.B. Ponton, and H.E. Evans, The Failure of Protective Oxides on Plasma-Sprayed NiCrAlY Overlay Coatings, *Oxid. Met.,* 2000, **53**(3-4), p 241-258
33. F.H. Stott, Influence of Alloy Additions on Oxidation, *Mater. Sci. Technol.,* 1989, **5,** p 734-740
34. Y.N. Wu, G. Zhang, Z.C. Feng, B.C. Zhang, Y. Liang, and F.J. Liu, Oxidation Behavior of Laser Remelted Plasma Sprayed NiCrAlY and NiCrAlY-Al_2O_3 Coatings, *Surf. Coat. Technol.,* 2001, **138,** p 56-60
35. X. Wu, D. Weng, Z. Chen, and L. Xu, Effects of Plasma-Sprayed NiCrAl/ZrO_2 Intermediate on the Combination Ability of Coatings, *Surf. Coat. Technol.,* 2001, **140,** p 231-237
36. Y. Longa-Nava and M. Takemoto, High-Temperature Corrosion of Laser-Glazed Alloys in Na_2SO_4-V_2O_5, *Corrosion,* 1992, **48**(7), p 599-607
37. U.K. Chatterjee, S.K. Bose, and S.K. Roy, *Environmental Degradation of Metals,* Marcel Dekker, 2001
38. Y. Longa-Nava, Y.S. Zhang, M. Takemoto, and R.A. Rapp, Hot Corrosion of Nickel-Chromium and Nickel-Chromium-Aluminum Thermal-Spray Coatings by Sodium Sulfate-Sodium Metavanadate Salt, *Corrosion,* 1996, **52**(9), p 680-689
39. G. Calvarin, R. Molins, and A.M. Huntz, Oxidation Mechanism of Ni-20Cr Foils and its Relation to the Oxide-Scale Microstructure, *Oxid. Met.,* 2000, **53**(1-2), p 25-48
40. H. Nickel, W.J. Quadakkers, and L. Singheiser, Analysis of Corrosion Layers on Protective Coatings and High Temperature Materials in Simulated Service Environments of Modern Power Plants Using SNMS, SIMS, SEM, TEM, RBS and X-Ray Diffraction Studies, *Anal. Bioanal. Chem.,* 2002, **374,** p 581-587
41. A. Ul-Hamid, Diverse Scaling Behavior of the Ni-20Cr Alloy, *Mater. Chem. Phys.,* 2003, **80,** p 135-142
42. B.S. Sidhu and S. Prakash, Evaluation of the Corrosion Behaviour of Plasma-Sprayed Ni_3Al Coatings on Steel in Oxidation and Molten Salt Environment at 900 °C, *Surf. Coat. Technol.,* 2003, **166**(1), p 89-100
43. A.U. Malik, R. Ahmad, S. Ahmad, and S. Ahmad, High Temperature Oxidation Behaviour of Nickel Aluminide Coated Mild Steel, *Pract. Metallogr.,* 1992, **29,** p 255-268
44. W.H. Lee and R.Y. Lin, Hot Corrosion Mechanism of Intermetallic Compound Ni_3Al, *Mater. Chem. Phys.,* 2002, **77,** p 86-96
45. G.J. Santoro, Hot Corrosion of Four Superalloys: HA-188, S-57, IN-617 and TD-NiCrAl, *Oxid. Met.,* 1979, **13**(5), p 405-435
46. K.L. Luthra, Kinetics of the Low Temperature Hot Corrosion of Co-Cr-Al Alloys, *J. Electrochem. Soc.,* 1985, **132**(6), p 1293-1298
47. N.S. Bornstein, M.A. Decrescente, and H.A. Roth, Effect of Vanadium and Sodium Compounds on the Accelerated Oxidation of Nickel Base Alloys, *Proc. Conf. on Gas Turbine Materials in the Marine Environment* (Columbus, OH), 1975, MMIC-75-27, p 115-160
48. Z. Liu, W. Gao, K.L. Dahm, and F. Wang, Oxidation Behaviour of Sputter-Deposited Ni-Cr-Al Micro-Crystalline Coatings, *Acta Mater.,* 1998, **46**(5), p 1691-1700
49. F.H. Stott, Developments in Understanding the Mechanisms of Growth of Protective Scales on High-Temperature Alloys, *Mater. Charact.,* 1992, **28**(3), p 311-325
50. W.Y. Chan, H.E. Evans, C.B. Ponton, J.R. Nicholls, and N.J. Simms, Influence of $NiAl_3$ on the High Temperature Oxidation of a Plasma-Sprayed Overlay Coating, *Mater. High Temp.,* 2000, **17**(2), p 173-178
51. A. Strawbridge, H.E. Evans, and C.B. Ponton, Spallation of Oxide Scales from NiCrAlY Overlay Coatings, *Mater. Sci. Forum,* 1997, **251-254,** p 365-374
52. R.A. Rapp, J.H. Devan, D.L. Douglass, P.C. Nordine, F.S. Pettit, and D.P. Whittle, High Temperature Corrosion in Energy Systems, *Mater. Sci. Eng.,* 1981, **50,** p 1-17
53. P.S. Liu, K.M. Liang, H.Y. Zhou, S.R. Gu, X.F. Sun, H.R. Guan, T. Jin, and K.N. Yang, Cyclic Oxidation Behavior of Aluminide Coatings on the Co-Base Superalloy DZ40M, *Surf. Coat. Technol.,* 2001, **145,** p 75-79